Disturbance and Response Time Improvement of Submicrometer Precision Linear Motion System by Using Modified Disturbance Compensator and Internal Model Reference Control

Hoi-Wai Chow, *Member, IEEE*, and Norbert C. Cheung, *Senior Member, IEEE*

***Abstract*—Permanent magnet linear motors are a type of linear motors that are generally used in precision motion control applications. However, the position of motor is easily disturbed by external force, disturbance, and variation in parameters of plant. Therefore, the construction of the high-precision linear motion system is a difficult task. This paper implements a modified disturbance observer and compensator, which includes a novel variable gain, to overcome the effects of unknown parameters of the motor, to minimize the effect of the disturbance, and to reduce the response time of the disturbance. This compensated linear motor is further controlled by the internal model reference control algorithm so that the position of the motor can be tracked with expected response precisely. The authors conducted the experiments and verified the feasibility of the high-precision positioning control. Compared with the case of normal disturbance compensator, the experimental results also illustrate the improvements of the novel variable gain, which reduces the response time toward the command signal and the external disturbance.**

***Index Terms*—Disturbance observer and compensator, internal model reference control (IMRC), permanent magnet linear motors (PMLMs).**

I. Introduction

THE permanent magnet linear motor (PMLM) is one of the preferred choices for the actuator of linear motor. PMLM has several benefits, such as no backlash, less friction, high thrust density, higher acceleration/deceleration capability, and low thermal losses. This motor has been widely employed in industrial applications, and some engineers have attempted to utilize PMLM to achieve a high-precision linear motion system by different control algorithms. For example, Park [1] implemented a hybrid stage motion system using precision motion controller which consists of a position, velocity control loop, and an antiwindup compensator. Seshagiri [2] proposed a "servocompensator" as part of a robust sliding-mode control of permanent magnet stepper motors. In [3], Cao and Low applied a new model predictive control approach on the PMLM with repetitive tracking tasks. It can effectively reduce the tracking error from friction and achieve the high-precision motion control from the periodic disturbance after 5–20 runs. In [6], Sung and Huang also implemented the optimal PI controller with modified integrator and genetic algorithm on the PMLM to develop a high-precision linear motion system.

The PMLM is usually decided and manufactured for general linear motion purpose instead of precision motion purpose. The accuracy of the motor position, however, can be easily affected by variations in parameters of motor and load disturbances, including the friction and the ripple force. In order to handle these disadvantages, many engineers focus on the estimation of variations or development of nonlinear disturbance model for the motion system. In [5], Hong and Yao proposed a nonlinear adaptive robust controller with saturated actuator for a PMLM, which is subject to parametric uncertainties and uncertain nonlinearities, guaranteed transient performance and final tracking accuracy, and identified parameter effectively. Huang and Sung [4] controlled the PMLM using a new function-based sliding-mode control method and direct thrust control to accomplish a high-precision linear motion system. They integrate the flux estimation to determine the magnitude and phase angle of the controlled motors so that they can solve the chattering, parameter variations, and external disturbance problems successfully. Authors in [7] also demonstrated a compensation scheme of force ripple based on a model of the disturbance. The compensation term in this method is applied in parallel to the position/velocity controller. Chen *et al.* [8] also developed a ripple and friction compensation scheme by using hysteretic relay.

Nevertheless, those solutions require strenuous mathematics calculation to estimate the plant parameters such as flux and phase angle so that the control signal could be generated for high-precision motion control. This tedious mathematics work will raise the system cost and controller design time. The inverse-model-based disturbance observer and compensator is a possible and effective method to eliminate those variations in parameters and disturbances, including the friction and the ripple force. The compensated linear motion system will become a linear model, and the control algorithm can be simpler. Some engineers also apply this attractive technique to control

Manuscript received March 10, 2011; revised August 10, 2011 and October 21, 2011; accepted January 7, 2012. Date of publication January 18, 2012; date of current version September 6, 2012.

H.-W. Chow is with the Power Electronic Laboratory, The Hong Kong Polytechnic University, Hung Hom, Hong Kong (e-mail: waison_chow_hk@yahoo.com.hk).

N. C. Cheung is with the Department of Electrical Engineering, The Hong Kong Polytechnic University, Hung Hom, Hong Kong (e-mail: norbert_cheung@polyu.edu.hk).

Color versions of one or more of the figures in this paper are available online at http://ieeexplore.ieee.org.

Digital Object Identifier 10.1109/TIE.2012.2185015

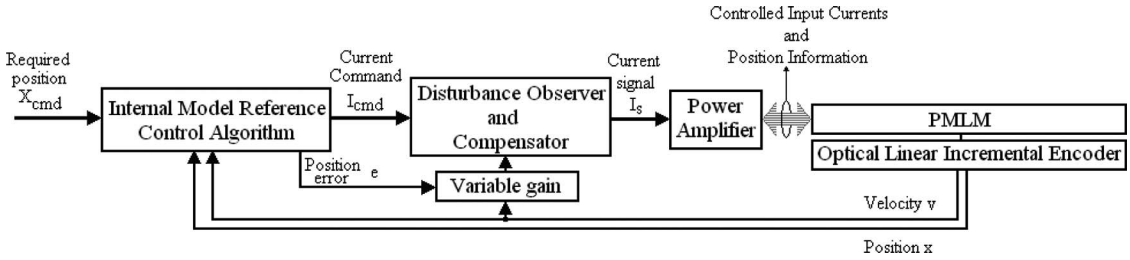

Fig. 1. Overall block diagram of the proposed linear motion system.

the PMLM. Yao *et al.* [9] proposed a controller with an inverse of the first-order reference model with an input deduction and integral term. It can reduce modeling uncertainty due to the unknown of real system and disturbance due to the $d-q$-axis coupling effect. Zhang *et al.* [10] integrated a friction-model-based feedforward approach and an inverse-model-based disturbance observer to develop a high-precision 2-D system with two linear motors. The developed systems successfully achieve a position error of less than 2 μm. In [11], Komada *et al.* developed a disturbance observer for PMLM driven under constant force operation to compensate the effect of parameter variation, friction, ripple force, and external disturbance force.

However, the described disturbance compensators usually focus on the compensation process and neglect the response time for the disturbance. In this paper, the disturbances on PMLM, including friction, ripple force, and load variation, are calculated by online measurements. These disturbances are then eliminated by a disturbance observer and compensator. The dynamics of the motor (velocity and position) are being controlled by an internal model reference control (IMRC) algorithm so that the outputs of the linear motor (velocity and position) can track the predefined trajectory. In addition, a variable gain is employed to modify the conventional compensator. The major contribution is introducing this variable gain into the conventional distribution observer and compensator. The impact of this gain is to improve the compensation for the transient disturbance. This is neglected by the conventional disturbance compensator. The gain can greatly reduce the response time on the disturbance and static friction. Another contribution of this paper is to develop a method to optimize the effect of low-pass filter (LPF) inside the observer.

II. Overview of the Project

The proposed control method for PMLM is shown in Fig. 1. A PMLM is driven by a power amplifier which is configured as current-driven mode. The velocity and the current command are utilized to estimate the actual disturbances, and this estimation is converted into a compensation current by the "disturbance observer and compensator." This disturbance compensator is a variable structure which is adjusted based on the position error and the operating speed so that the response time on the disturbance can be further improved. The compensated PMLM (disturbance-free motion system) is controlled by the "IMRC algorithm" with feedback velocity and position. The detail of each part will be introduced in the following sections.

III. Design of Disturbance Compensation

If the PMLM motor is driven under a rated speed, the direct axis current is equal to zero, the motor will be operated at the constant force operation [12], and the thrust force $F_{\rm em}$ from the motor can be calculated by

$$F_{\rm em} = K_f \times I_s. \tag{1}$$

K_f and I_s in (1) are the force constant and current injected to the motor. Equation (1) can also act as the model of PMLM. Although the structure of this model is very simple, many engineers [11], [13]–[15] also employed (1) during the controller design and achieved the high-precision motion control. Typically, the direct drive motion system is directly affected by external disturbances $F_{\rm dis}$. In other words, this nonlinear $F_{\rm dis}$ perturbs the outputs of the PMLM (velocity v and position x) directly. $F_{\rm dis}$ includes load variation, force ripple, and some unexpected external disturbance. $F_{\rm em}$ needs to overcome $F_{\rm dis}$ and friction to drive the translator of the PMLM. This is an important issue particularly concerned in precision motion control system.

Note that the conventional disturbance compensation method was adopted by many engineers. References [11], [16], and [17] are some examples using this disturbance compensator to achieve high-precision linear motion control. In this paper, this conventional method is modified to form a new compensator. The design process and the operating principle of a conventional disturbance compensator are therefore first reviewed in detail.

A. Operation of Conventional Disturbance Observer and Compensator

In order to minimize the effect of perturbation on PMLM, the "disturbance observer and compensator" is proposed in this project. This observer and compensator is based on the idea mentioned in [11]. The structure of the disturbance observer and compensator is shown in Fig. 2(a). If the equation of the "plant" is formulated, the relationship between I_s and v will be arranged as

$$I_s(\Delta K_f + K_{fn}) - F_{\rm dis} = (M_n s + \Delta M s + D)v. \tag{2}$$

M is the mass of the translator of the PMLM, which is the sum of the nominal mass M_n and the mass deviation ΔM. K_f is the force constant, which is the sum of the nominal force constant K_{fn} and the force constant deviation ΔK_f. D is the frictional constant. The nominal parameters (M_n and K_{fn}) can

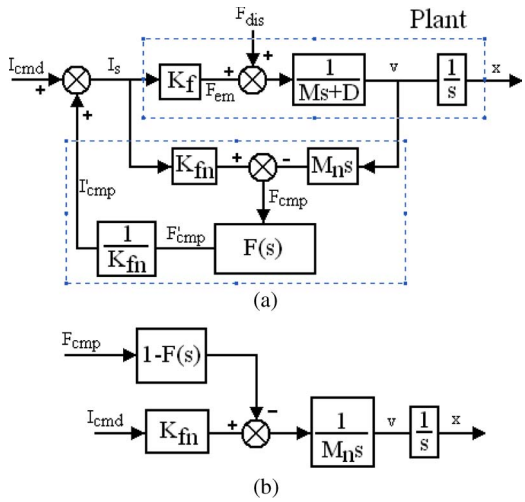

Fig. 2. (a) Block diagram of motion system with disturbance observer and compensator. (b) Simplified block diagram of motion system.

be obtained from the datasheets, and they usually have slight deviations from their actual values (M and K_f).

If all nonlinear disturbances, friction, and deviation terms are grouped together, (2) can be rearranged as

$$F_{\text{cmp}} = \Delta M sv + Dv - I_s \Delta K_f - F_{\text{dis}} = I_s K_{fn} - M_n sv. \quad (3)$$

External disturbances F_{dis}, kinetic frictional force Dv, and parameter variation $\Delta M sv - I_s \Delta K_f$ are grouped as a term called the compensation force F_{cmp}, which can be calculated by measuring I_s and v. In fact, this F_{cmp} has to be compensated so that the PMLM can be operated as an ideal model given as

$$I_{\text{cmd}} = \frac{M_n}{K_{fn}} sv. \quad (4)$$

Compared with the compensator in [11], the new proposed compensator in this paper also compensates the term Dv, which is not totally rejected by the method in [11].

Since F_{cmp} is calculated by the derivative of velocity dv/dt, an LPF has to be inserted to suppress the high-frequency noise in F_{cmp}. The function of LPF is named as $F(s)$. The filtered estimation F'_{cmp} is then converted into the compensation current I'_{cmp} by multiplying a gain $1/K_{fn}$. I'_{cmp} is fed back to the thrust current I_s so that all low-frequency disturbances and frictional force are compensated.

With the presence of LPF, the equation of the compensated PMLM will become (5), which is modified from (3). The block diagram of the system is shown in Fig. 2(b).

$$\left(I_{\text{cmd}} + \frac{1}{K_{fn}} F(s) F_{\text{cmp}}\right) K_{fn} - M_n sv = F_{\text{cmp}}$$
$$I_{\text{cmd}} K_{fn} - M_n sv = [1 - F(s)] F_{\text{cmp}}. \quad (5)$$

B. Novel Modification for Disturbance Compensation

The disturbance compensation algorithms mentioned in the previous sections are the standard disturbance compensator. In fact, the high-precision positioning control can be achieved effectively by only using the standard algorithms. However, the

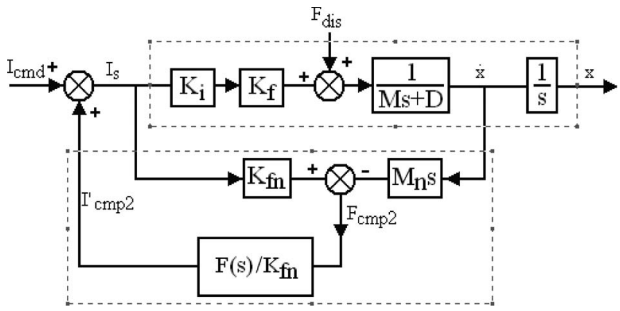

Fig. 3. Modified disturbance compensator for PMLM.

high-frequency components of F_{cmp} still perturb the outputs of the "disturbance-free" PMLM. The main source of the high-frequency components of F_{cmp} is the presence of static friction. This section explains the transient disturbance and proposes a novel modification for a conventional disturbance compensator. This modification further improves the PMLM to be the ideal system in (4). The achievement of high-precision linear motion system can be easier.

Considering the original compensated PMLM shown in (5), the term $[1 - F(s)] \times F_{\text{cmp}}$ appears, and it is the high frequency of F_{cmp}. Fortunately, the major components of F_{cmp} are usually at low frequency, and they can be compensated. However, the transient disturbances, which are high-frequency components, will still affect the outputs of the PMLM. Examples of transient disturbances are sudden external impact and static friction. A novel modification, inserting an additional extra gain K_i, is applied to the conventional disturbance compensator. The modified compensation block diagram can be modified as shown in Fig. 3. Considering the compensated PMLM with K_i, the equations of the plant can be derived as

$$I_s K_i (K_{fn} + \Delta K_f) + F_{\text{dis}} = (M_n s + \Delta M s) v + Dv. \quad (6)$$

This PMLM with K_i can be rearranged as shown in (7), and those perturbations appearing in this PMLM are grouped and named as F_{cmp2}.

$$\begin{aligned} I_s K_{fn} - M_n sv &= F_{\text{cmp2}} \\ &= \Delta M sv + Dv - F_{\text{dis}} \\ &\quad - I_s K_i \Delta K_f - I_s K_{fn} (K_i - 1). \end{aligned} \quad (7)$$

If this F_{cmp2} is converted to a compensation current I'_{cmp2} and fed back to the PMLM, the equations of the compensated system can be rearranged as

$$I_{\text{cmd}} K_{fn} - M_n sv = [1 - F(s)] F_{\text{cmp2}}. \quad (8)$$

Equation (8) can be rearranged into two structures shown in (9) and (10). They can be used for explaining the properties of the new disturbance compensated system.

$$\begin{aligned} I_{\text{cmd}} K_{fn} - M_n sv &= [1 - F(s)] \\ &\quad \times [F_{\text{cmp}} - I_s K_f (K_i - 1)] \quad (9) \\ I_{\text{cmd}} K_{fn} - M_n sv &= (\Delta M sv + Dv - F_{\text{dis}} - I_s \Delta K_f K_i) \\ &\quad \times [1 - K_i F(s)] - I_{\text{cmd}} K_{fn} (K_i - 1) \\ &\quad \times [1 - K_i F(s)] \\ &\quad + I'_{\text{cmp2}} K_{fn} (K_i - 1) F(s). \quad (10) \end{aligned}$$

The equation format of (8) is the same as (5). This means that the modified system in (8) can also reject the external disturbance force, kinetic friction, and parameter variation. The merit of the modified compensator can be observed from (9). Equation (9) is rearranged for comparison with (5). An additional term $[1 - F(s)] \times [I_s K_f (K_i - 1)]$ has appeared in (9). Since the term $1 - F(s)$ has a high-pass filtering characteristic, this additional term can calculate the high-frequency components of I_s which is composed of the input current command $(I_{\rm cmd})$ and the compensation current for $F_{\rm cmp2}(I'_{\rm cmp2})$. In other words, when the command or disturbance changes suddenly, the high-frequency components of I_s will be larger, and extra efforts will be added to the PMLM. The modified systems will respond to the high-frequency disturbances, such as impulse disturbance, faster than the conventional compensation system because of the presence of $I'_{\rm cmp2}$. In addition, the modified systems will respond to the current command $I_{\rm cmd}$ faster because I_s includes $I_{\rm cmd}$. The gain K_i will amplify the high-frequency components of $I_{\rm cmd}$ and produce additional effort to drive the PMLM to command inputs.

Inserting K_i can reduce the adverse effect of static friction. Considering the conventional compensation method shown in Fig. 2, when the velocity of the PMLM is crossing zero (the translator reverses its direction or starts moving from rest), the motor may remain stationary (velocity remains zero) even if there is current injected to the motor because of the presence of static friction. Since there is a difference between the expected thrust force $(I_s K_{fn})$ and the actual thrust force $(M_n sv = 0)$, the $F_{\rm cmp}$ will rise quickly, and the effect of static friction will be reflected in $I'_{\rm cmp}$. This $I'_{\rm cmp}$ is fed back to the translator and eliminates the effect of static friction after a short period of time. Note that the effect of static friction is like a transient force stopping the motor and it belongs to high-frequency disturbance. Now, referring to the new compensated PMLM in (9), $[1 - F(s)] \times [I_s K_f (K_i - 1)]$ can provide extra effort to eliminate the static friction because I_s contains $I'_{\rm cmp2}$. The time for eliminating the static friction should be shorter compared with the PMLM with a conventional disturbance compensator.

Inserting K_i is a possible suggestion for reducing the transient effect of disturbance and command, but it will also cause some adverse effects to the output of PMLM if K_i is not chosen carefully. The term $[1 - F(s)] \times [I_s K_f (K_i - 1)]$ contains a high-pass filter $1 - F(s)$, and it does not only pass the high-frequency components of I_s but also allows the noise in $F_{\rm cmp2}$ to be injected to the PMLM. The level of noise will be amplified, and this causes oscillation and audible noise if K_i is too large.

Equation (10) is the other form of the new compensated PMLM, and it can be utilized to determine the maximum and minimum values of K_i. The right-hand side of this equation consists of three terms. The first term is related to the effect of parameter variation, kinetic friction, and $F_{\rm dis}$. The second term is related to $I_{\rm cmd}$, and the final term is related to $I'_{\rm cmp2}$. In this equation, there is a variable filter $(1 - K_i F(s))$ with special characteristic. Its magnitude plot with different K_i is obtained as shown in Fig. 4. When K_i is smaller than two, this filter has the high-pass filtering characteristics. When K_i is equal to or larger than two, the filter will amplify the signal, instead of suppressing the signal, because its magnitude is always larger than 0 dB. The first term in (10) is expected to be suppressed, so K_i should not be larger than two. Meanwhile, if K_i is smaller than one, the response rate of the plant will be deteriorated. Note that the second and third terms are the high-pass-filtered $I_{\rm cmd}$ and exceeding $I'_{\rm cmp2}$. These two currents provide extra efforts to improve the dynamic response of the PMLM.

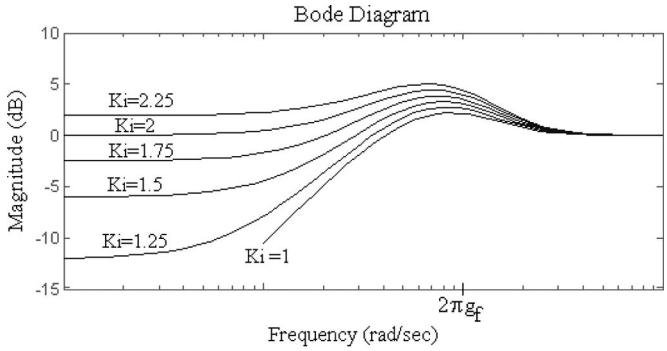

Fig. 4. Magnitude plot of transfer function of $1 - K_i F(s)$ with different K_i.

For the practical situation, the effect of high-frequency disturbance will dominate when the translator is near the targeted position and travels at low velocity. Hence, the proposed additional gain K_i is designed with the following considerations.

1) When the position error is small and the translator is slow, K_i is selected to be two.
2) For other cases, the motor is operating at normal condition, which means that K_i is selected to be one.

However, the profile of K_i should be determined by experiments, and it will be discussed later.

C. LPF Design Criteria

The design of LPF is a critical process of constructing the "disturbance observer and compensator" since the selection of cutoff frequency of LPF will directly influence the performance of compensation. There are four criteria to determine the value of cutoff frequency g_f.

1) The main function of the LPF is to filter the noise in $I_s K_f n - M_n sv$ which mainly comes from the differentiation of velocity. The frequency of noise in acceleration will be $f_{\rm sampling}/2$, where $f_{\rm sampling}$ is the sampling frequency of the DSP. The cutoff frequency of LPF should be much smaller than $f_{\rm sampling}/2$ (i.e., $g_f < \pi \times f_{\rm sampling}$).
2) Considering the input of LPF $(I_s K_f n - M_n sv)$, the cutoff frequency of LPF should not be smaller than the operating frequency of the PMLM system. Otherwise, the LPF will distort the useful information in this input. In other words, the $g_f/2\pi$ should be higher than the operating frequency of the PMLM system.
3) Since the LPF is inserted into the observer and compensator, the model of compensated PMLM will become the system shown in (5) and (8). $1 - F(s)$ in these two equations is a high-pass filter, and only high-frequency components of $F_{\rm cmp}$ and $F_{\rm cmp2}$ can perturb the outputs of the PMLM. $g_f/2\pi$ should be slightly higher than all

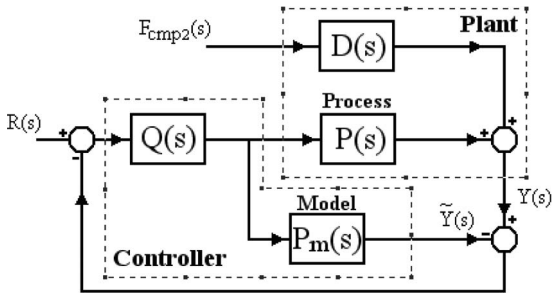

Fig. 5. Diagram for IMRC.

dominant components of $F_{\rm cmp}$ and $F_{\rm cmp2}$ in order to suppress the effect of $F_{\rm cmp}$ and $F_{\rm cmp2}$.

4) Another restriction of g_f is caused by the "power amplifier" of the PMLM. Under the current control mode, there is a current feedback loop inside the power amplifier, and the current loop will have its own cutoff frequency. The $g_f/2\pi$ should be smaller than this cutoff frequency.

The LPF implemented in this project is a third-order critical damping LPF given as

$$F(s) = \left(\frac{1}{\frac{1}{g_f}s + 1}\right)^3. \tag{11}$$

It is expected that the noise amplitudes of $F_{\rm cmp}$ and $F_{\rm cmp2}$ are very large and the third-order filter can provide a higher cutoff frequency and high ability of noise suppression. Although there are many different forms of third-order LPF, the authors prefer using the aforementioned structure in order to simplify the process modifying g_f during the experiment. In this project, the possible range of g_f is quite wide, and the critical value must be determined experimentally.

IV. IMRC

The IMRC algorithm [18]–[20] has been proposed for many decades, but it is seldom employed in high-precision motion control. It is because this algorithm could not compensate the nonlinearity of external disturbances and parameter uncertainties in the model. In this paper, the IMRC integrates with the disturbance observer and compensator so as to develop a generic controller for PMLM to accomplish the high-precision linear motion system.

A. Operation of IMRC

IMRC can be explained by Fig. 5. $P(s)$ stands for the actual process of the system. $D(s)$ stands for disturbance transfer function. The controller of this algorithm is constructed by designable transfer function $Q(s)$ and the model of process $P_m(s)$. The output of the plant is $Y(s)$, and it is formulated as

$$Y(s) = \frac{P(s)Q(s)R(s) + (1 - P(s)Q(s))\,D(s)F_{\rm cmp2}(s)}{1 + (P(s) - P_m(s))\,Q(s)}. \tag{12}$$

If the model is exactly equal to the process, i.e., $P_m(s) = P(s)$, the denominator of $Y(s)$ will be equal to one. In addition, if $D(s)F_{\rm cmp2}(s)$ is suppressed or compensated to zero, the overall output of the controlled system in (12) will be modified to a simple mathematical equation as shown in (13). Since $Q(s)$ is freely designed, it can be designed as in (14).

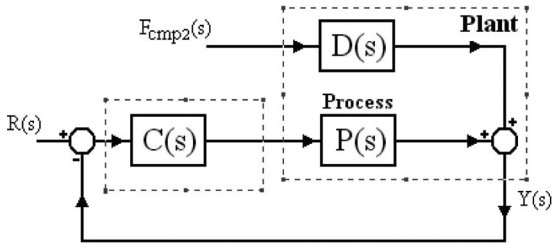

Fig. 6. Simplified for IMRC.

$$Y(s) = P(s)Q(s)R(s) \tag{13}$$

$$Q(s) = \frac{1}{P_m(s)}M(s) \Rightarrow Y(s) = M(s)R(s). \tag{14}$$

$M(s)$ is the predefined model, and $R(s)$ is the input function. The output $Y(s)$ becomes a predefined trajectory $M(s)R(s)$. Note that another function of $M(s)$ is to ensure that the transfer function $Q(s)$ is proper. Therefore, the order of $M(s)$ should be equal to or higher than that of $P_m(s)$. In addition, $P(s)$ and $P_m(s)$ should be the minimum-phase system.

Referring to Fig. 5, the controller is composed of the system model $P_m(s)$ and the transfer function $Q(s)$. They can be combined to produce a feedback controller $C(s)$ by (15), and the rearranged block diagram is shown in Fig. 6.

$$C(s) = \frac{Q(s)}{1 - P_m(s)Q(s)}. \tag{15}$$

B. Implementation of IMRC for PMLM

In this project, this control approach is applied to the PMLM for the high-precision linear motion control. A cascaded structure controller with position and velocity feedback is proposed so that the velocity loop and position loop can be modified independently. The formulas required in the IMRC are summarized as shown in Table I. Since the model of PMLM has been already derived as shown in (4), the IMRC control algorithm for the velocity loop can be formulated easily. The controlled PMLM will be a system $P_v(s)$ with the input equal to the required current command $I_{\rm cmd}$ and the output equal to the velocity of the motor v. The model of the controlled process can be formulated as $P_{mv}(s)$. The first-order predefined model $M_v(s)$ is used, and the proposed transfer function for $Q_v(s)$ is therefore constructed. $1/g_v$ in $M_v(s)$ and $Q_v(s)$ is the time constant of the predefined model, and it will limit the frequency of the velocity loop.

The IMRC can be further applied to control the position of PMLM. Consider the process with the position output $P_p(s)$, which has the velocity command $v_{\rm cmd}$ as input and the position x as output. Similar to the velocity loop, the transfer function $P_{mp}(s), M_p(s), Q_p(s)$ can be formulated. Note that the predefined model for position loop $M_p(s)$ is designed as a second-order function because the $P_{mp}(s)$ is a second-order system. The time constant $1/g_x$ limits the frequency of the position loop.

TABLE I
FORMULAS FOR IMRC

	Velocity Loop	Position Loop
Model of the plant	$P_{mv}(s)=\frac{V(s)}{I_{cmd}(s)}=\frac{K_{fn}}{M_n s}$	$P_{mp}(s)=\frac{X(s)}{V_{cmd}(s)}=\frac{1}{s}\times\frac{1}{\frac{s}{g_v}+1}$
Reference model	$M_v(s)=\frac{1}{\frac{s}{g_v}+1}$	$M_p(s)=\frac{1}{\left(\frac{s}{g_x}+1\right)^2}$
Function $Q(s)$	$Q_v(s)=\frac{M_v(s)}{P_{mv}(s)}=\frac{M_n s}{K_{fn}\left(\frac{s}{g_v}+1\right)}$	$Q_p(s)=\frac{M_p(s)}{P_{mp}(s)}=\frac{s}{\left(\frac{s}{g_x}+1\right)}$
Combined Controller	$C_v(s)=\frac{M_n g_v}{K_{fn}}$	$C_p(s)=\frac{\frac{1}{g_v}s+1}{\frac{1}{g_x^2}s+\frac{2}{g_x}}$

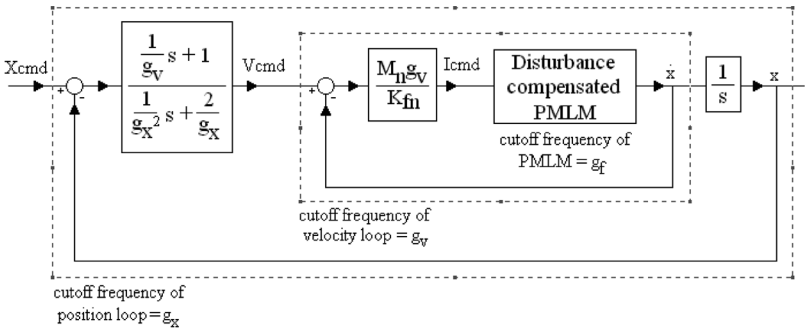

Fig. 7. Block diagram for entire control algorithm.

In order to simplify the structures of the controllers in both loops, the $Q(s)$ and $M(s)$ are combined to formulate $C_v(s)$ and $C_p(s)$. The overall control algorithm is shown in Fig. 7.

C. Stability of the Controlled PMLM With IMRC

Considering the entire system of new compensated PMLM with IMRC controllers, the position output equation can be derived as

$$X = X_{\rm cmd}\frac{1}{\left(\frac{1}{g_x}s+1\right)^2} - F_{\rm cmp2}\left[\frac{\left[\left(\frac{1}{g_f}s+1\right)^3-1\right]\left(\frac{1}{g_x^2}s+\frac{2}{g_x}\right)}{\left(\frac{1}{g_f}s+1\right)^3(M_n s+M_n g_v)\left(\frac{1}{g_x}s+1\right)^2}\right] \quad (16)$$

$$X = X_{\rm cmd}H_1(s) - F_{\rm cmp2}H_2(s). \quad (17)$$

The stability of (16) can be ensured by studying the locations of poles of $H_1(s)$ and $H_2(s)$. All the poles of $H_1(s)$ and $H_2(s)$ appear at the left-hand side of the s-plane. The linear motion system controlled by IMRC is, therefore, a stable system. Note that $F_{\rm cmp2}$ is bounded and will be shown by experiment. Regarding the effect of K_i on the stability of outputs, as mentioned in Section III-B and (10), if K_i is smaller than two, the disturbances will not be amplified, and $F_{\rm cmp2}$ will also remain bounded. Overall, the system outputs will be stable if K_i is not larger than two.

V. HARDWARE IMPLEMENTATION AND RESULTS OF DISTURBANCE COMPENSATION AND IMRC

In order to investigate the actual performance of the proposed control method and algorithm, the experimental setup shown in Fig. 1 was connected. The linear motor used in this project was a PMLM (Servotube Module, SM1104, Copley Control

Corporation) which was driven by a servo driver (digital servo drive, ADP-090-09-S, Copley Control Corporation). The position sensor installed on the actuator was a linear incremental optical encoder (linear incremental optical encoder with 50-nm resolution, RGH24H30D30A, Renishaw). The terminals of the optical linear incremental encoder and the current input terminal in the amplifier were connected to a DSP (dSPACE Digital Signal Processing PCI board with $f_{\text{sampling}} = 20$ kHz, model no: dSPACE-1104). This powerful DSP allows the user to input the control algorithms through the simulink of MATLAB. The algorithms in time-continuous format (in s-domain) were transformed to the program code and uploaded to the real-time processor inside the DSP. During the experiment, the results and data can be stored by the DSP and plotted out for presentation. Note that the maximum current from the amplifier is 3 A and the maximum measurable speed of the encoder is 0.35 $\text{m} \cdot \text{s}^{-1}$.

The new proposed disturbance compensator is based on the conventional disturbance compensator, so the first step of experiment was to develop a compensated PMLM as shown in (5). g_f was determined and optimized experimentally. The IMRC control algorithms for the velocity loop and position loop were implemented. The performances of this compensated and controlled PMLM were studied. The results were recorded for comparison with the new proposed method.

With the help of IMRC, the position and the velocity of the PMLM can be controlled. The effects of K_i on the PMLM were investigated. The PMLM was driven with different command inputs and different K_i. The performances of the new proposed system were studied. The shape of K_i was then determined based on these results. With the optimized profile of K_i, the new proposed method was implemented. The performances of compensated PMLM with the new method were also investigated, and the results were studied.

A. Disturbance and Parameter Perturbation Measurement

As mentioned in Section I, many textbooks and engineers have already discussed and pinpointed the major difficulties of using PMLM to achieve a precision linear motion system. The difficulties include variations in parameters of motor, load disturbances, unexpected external disturbance force, friction, and the ripple force. Instead of handling the difficulties one by one, they are estimated and compensated by a single process.

An experiment to observe the disturbance in the PMLM at different position was conducted. The disturbances acting on the translator of the PMLM were measured, while the translator was commanded to travel forward and backward slowly. This experiment was repeated with two different velocities. The estimated disturbances are shown in Fig. 8. The disturbance acting on the PMLM was very complicated and not easy to be decomposed. In addition, if the traveling speed of the motor is adjusted, the curve of disturbance will change accordingly. Note that the measured disturbances are given by a lower curve and an upper curve. They were obtained when the motor traveled in the positive direction and the negative direction, respectively.

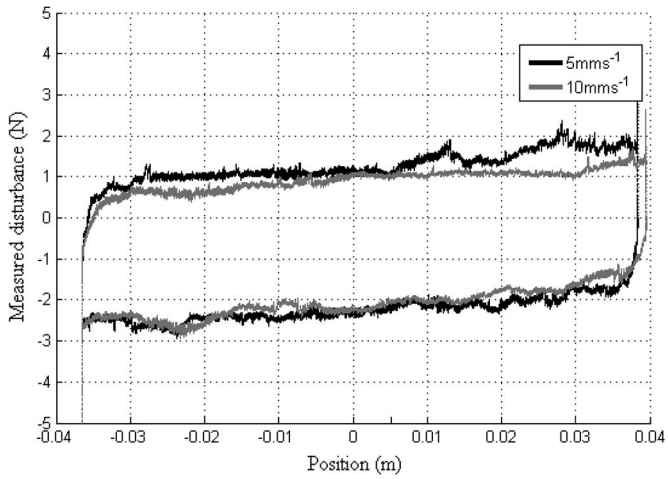

Fig. 8. Measured disturbance of noncompensated PMLM.

B. Conventional Disturbance Compensation

The "disturbance observer and compensator" shown in Fig. 2 was constructed. Referring to the original disturbance compensation algorithm, there is one parameter, g_f, which needed to be determined. The constraints in Section III-C are investigated.

1) The minimum amplitude of noise in F_{cmp} can be roughly deduced from the resolution of the optical incremental encoder. The resolution of the measured acceleration is 20 $\text{m} \cdot \text{s}^{-2}$. Based on (3), $F_{\text{cmp}} = (I_{\text{cmd}} + I'_{\text{cmp}})K_{fn} - M_n sv$, the minimum deviation in F_{cmp} will be $M_n \times 20 = 9$ N. The deviation in nonfiltered compensated current F'_{cmp}/K_{fn} is $9/4.1 = 2.195$ A. If this current deviation is injected to the PMLM, the audible noise and high-frequency oscillation in the position of PMLM will result. The frequency of this noise can be calculated by f_{sampling}/π. The cutoff frequency $g_f/2\pi$ should be smaller than this value.
2) The operation frequency of the positioning system was designed to be 25 Hz. It is the general operation frequency in many industrial applications. $g_f/2\pi$ should be much greater than 25 Hz.
3) Based on the measurement of disturbance shown in Fig. 8, the disturbances and perturbations are related to the position and the velocity. This means that the frequency of F_{cmp} or F_{cmp2} is also related to the operating frequency of the system. Thus, $g_f/2\pi$ should be much greater than 25 Hz.
4) The cutoff frequency of the current driver of PMLM is 3.2 kHz. The maximum value of g_f will be $2\pi \times 3200$. However, g_f should be much smaller than $2\pi \times 3200$ because the LPF has to suppress the noise in estimated F_{cmp}.

The possible range for g_f is also wide. In order to optimize g_f and achieve the high-speed compensation and the noise suppression, the performances of disturbance compensators with different g_f were investigated through the experiments.

The square wave current commands (with different amplitudes ranging from 0.1 to 0.35 A, with period equal to 0.4 s) were inputted to the disturbance compensated PMLM. The waveforms of compensated currents I'_{cmp} were recorded. The

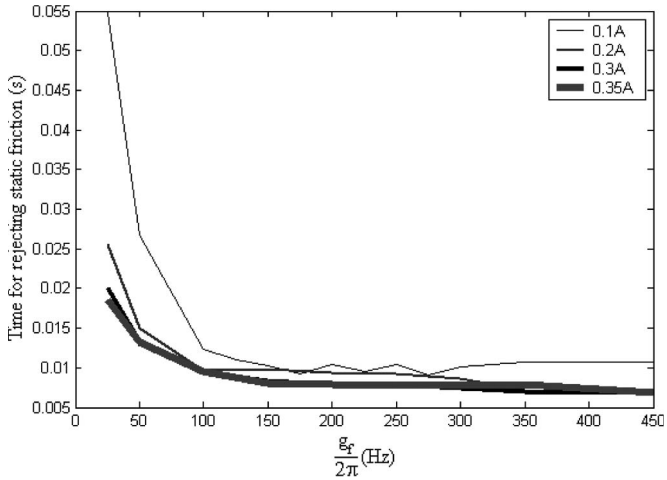

Fig. 9. Time to override static friction versus g_f.

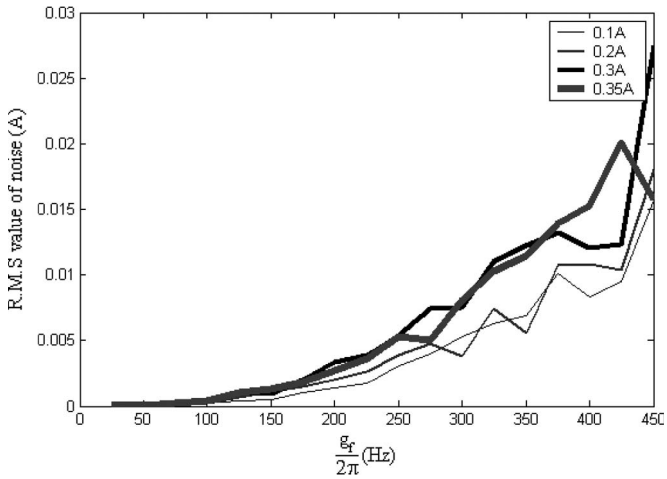

Fig. 10. RMS value of noise in $I_{\rm cmp}$ versus g_f.

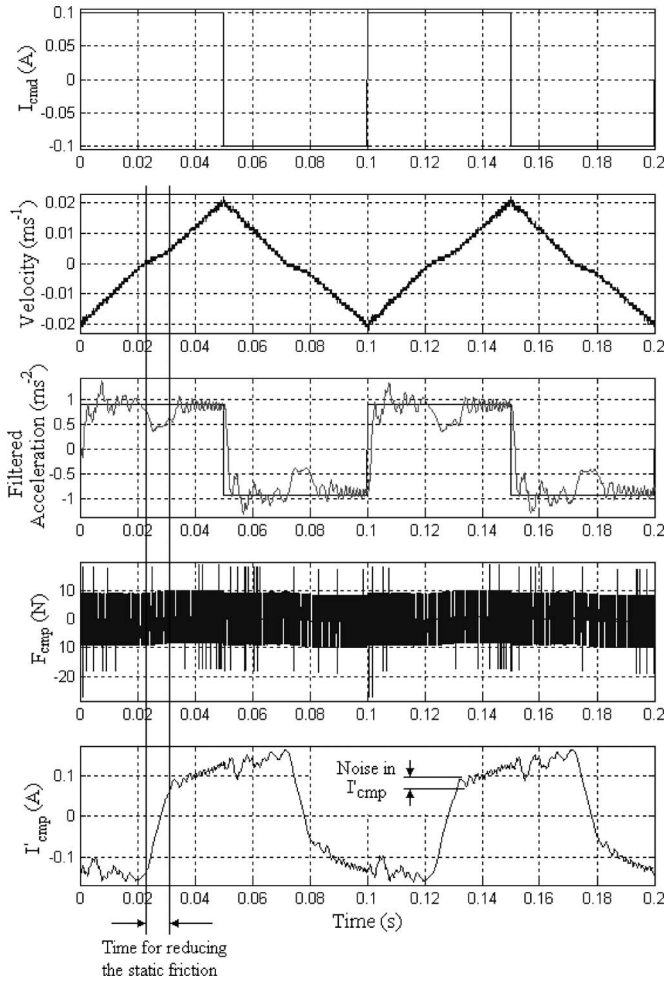

Fig. 11. Experimental results for performance of disturbance compensator with 0.1-A step input amplitude.

times of rejecting the static friction were obtained, and the rms values of the noise in $I'_{\rm cmp}$ were also recorded. The aforementioned experiments were repeated with different g_f. During the experiment, when g_f was larger than $2 \times \pi \times 450$, the PMLM generated audible noise, and this value was treated as the maximum limitation of g_f. The relationship between g_f, rejecting time, and rms value of noise was studied, and their plots are shown in Figs. 9 and 10.

It is obvious that the times of eliminating the static friction generally decrease with the g_f while the rms values of noise increase with g_f. There should be a tradeoff point optimizing the performance of the disturbance compensator. Regarding the times of rejecting the static friction, larger g_f can reduce the time. However, the effect of time reduction is not significant when g_f is larger than $2 \times \pi \times 150$. That means the minimum value of g_f should be $2 \times \pi \times 150$. Considering another plot related to the noise of $I'_{\rm cmp}$, the implication from this plot is that g_f has to be kept at a small value in order to minimize the noise level. No specific indication in this plot can define the maximum value of g_f.

Another condition can help to determine the value of g_f. Based on the common practice, the cutoff frequency of inner loop should be at least three times larger than that of the outer loop. The ratios between g_f, g_v, and g_x (cutoff frequency of different controlled loops) have to satisfy the following relationship:

$$g_f > 3 \times g_v > 9 \times g_x. \tag{18}$$

Since the expected operating frequency of a PMLM system is 25 Hz, g_x should be $2 \times \pi \times 25$. In this paper, g_f is chosen to be $2 \times \pi \times 250$.

To further investigate the performance of the disturbance compensator with $g_f = 2\pi \times 250$, an experiment was performed with a square wave current command (amplitude equal to 0.1 A). The experimental results are shown in Fig. 11. Based on the $I_{\rm cmd}$–time, velocity–time, and acceleration–time graphs, the function of disturbance compensator is achieved. The results agree with the ideal model shown in (4) except when the velocity is nearly zero. This difference is due to the presence of static friction. At that moment, the disturbance compensator has detected the static friction. $I'_{\rm cmp}$ will increase or decrease with a short period of time, which aims to reject this static friction. The response time of the compensator results in a difference between the ideal model shown in (4) and the actual performance. Referring to Fig. 11, the value of acceleration drops to zero when the speed is around zero. This phenomenon

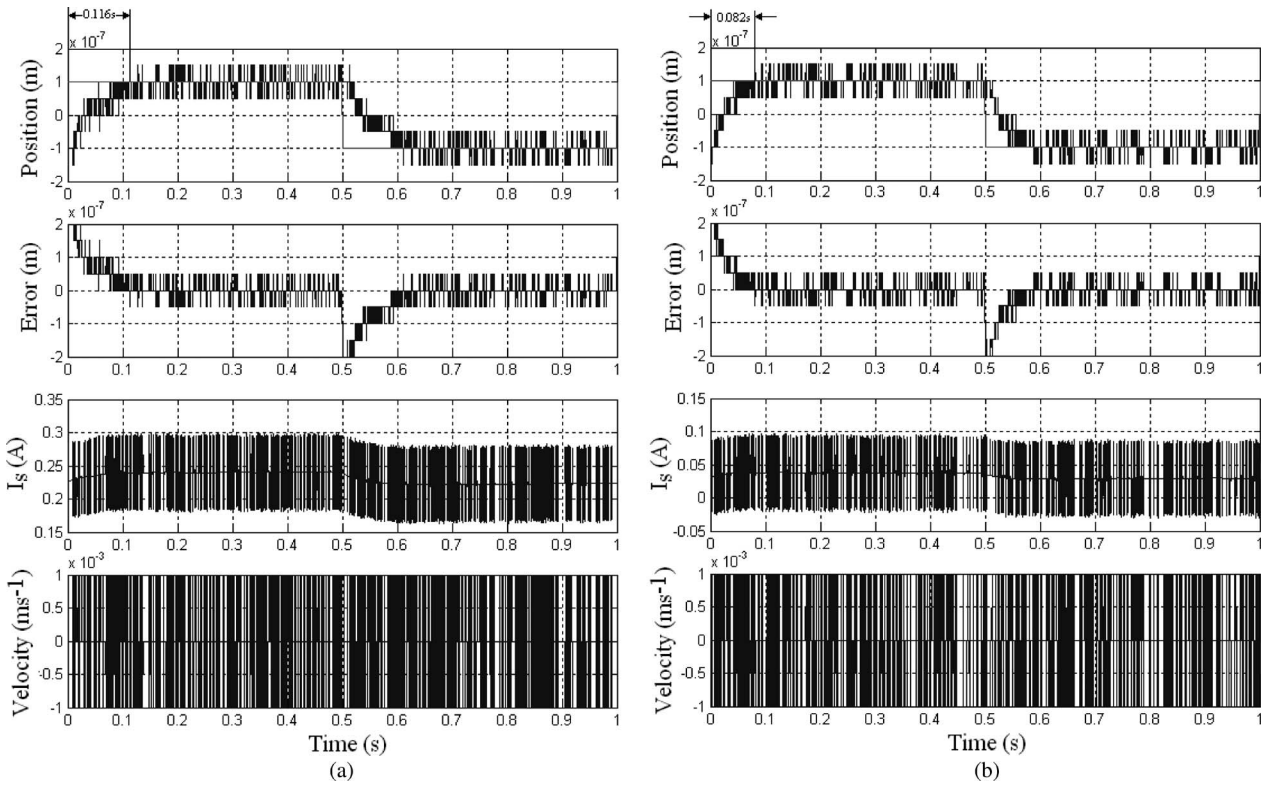

Fig. 12. Experimental results of controlled PMLM by standard IMRC algorithm (minimum step, with amplitude of square wave = 100 nm).

is also caused by the static friction. Note that the acceleration shown in Fig. 11 is filtered acceleration since the original noise of calculated acceleration is too large.

Another observation is related to the performance of the filter $F(s)$. The noise in $I_{\rm cmp}$ will be very high if there is absence of $F(s)$. This can be observed in $F_{\rm cmp}$. The presence of a third-order LPF can greatly reduce the noise amplitude to 0.01–0.02 A and provide effective disturbance compensation.

C. IMRC

The IMRC controller shown in Table I is implemented. Since g_f is selected as $2 \times \pi \times 250$, the value of g_v and g_x can be defined as $2 \times \pi \times 80$ and $2 \times \pi \times 25$, respectively. With these two parameters, the IMRC controller with cascaded structure was constructed. Two experiments of step responses (with minimum step and critical condition step) were performed. Their experimental results are shown in Figs. 12(a) and 13(a). The minimum step means that the step amplitude is one deviation of position error (equal to two resolutions of the optical linear incremental encoder $= 100$ nm). The critical condition step refers to the current or velocity of PMLM near saturation or reaching the maximum value. Another experiment illustrating the response time on external disturbance was also performed, and the results are shown in Fig. 14(a).

Although the compensated PMLM with IMRC algorithm can achieve the submicrometer precision linear motion system (with steady-state deviation equal to 100 nm), the performance of this linear motor is still not satisfactory. The major problem of the conventional method is the rising time of the position output. The rising time of controlled position output should be 0.05 s. However, the rising time of the minimum step response, shown in Fig. 12(a), is 0.116 s. This long rising time phenomenon is caused by the static friction and slow response rate of the disturbance compensator. Considering the overall control algorithm shown in Fig. 7, when the translator is commanded to move a very small distance, the position error is very small [error is ± 0.2 mum, as shown in Fig. 12(a)]. The gains of $C_p(s)$ and $C_v(s)$ should be about 63 and 55.2, respectively. The peak transient current calculated from the position error will be 0.696 mA. It is a very small current and definitely too small to overcome the static friction and drive the translator to move. Although the $I_{\rm cmd}$ (0.696 mA) is not large enough to drive the translator, the $I'_{\rm cmp}$ can assist the motor to overcome the static friction. If the I_s–time graph in Fig. 12(a) is considered, this current contains low-frequency components, which is exponentially rising and falling (in fact, it is $I'_{\rm cmp}$). This $I'_{\rm cmp}$ is accumulating slowly to overcome the static friction. In other words, the response time of the system is slow because of the rising time in I_s. Note that the problem of long settling time in position output is particularly serious when the position input command is too small.

Referring to the experimental results of critical step response, shown in Fig. 13(a), it is obvious that the peak current is 3 A and reaching its maximum value. Compared with the velocity of the translator, the current I_s reaches its limit much faster. This phenomenon is due to the fact that g_f is larger than g_v.

The rising time shown in Fig. 12(a) is smaller than that in Fig. 13(a). It is because larger $I_{\rm cmd}$ can provide larger effort to trigger the translator to move and overcome the static friction. This explanation can be supported by the I_s–time graph. If the step size is larger, the $I_{\rm cmd}$ will dominate in I_s. When the

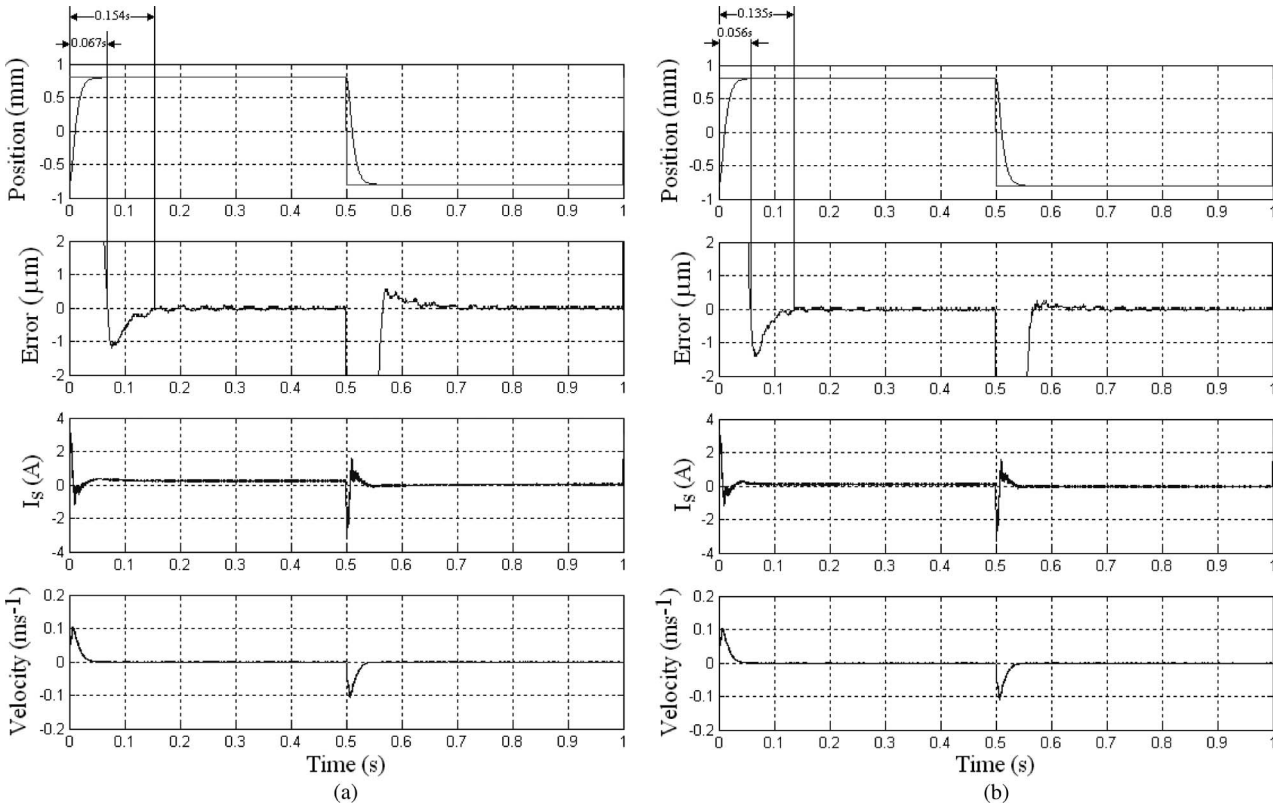

Fig. 13. Experimental results of controlled PMLM by standard IMRC algorithm (critical situation step, with amplitude of square wave $= 800\ \mu$m).

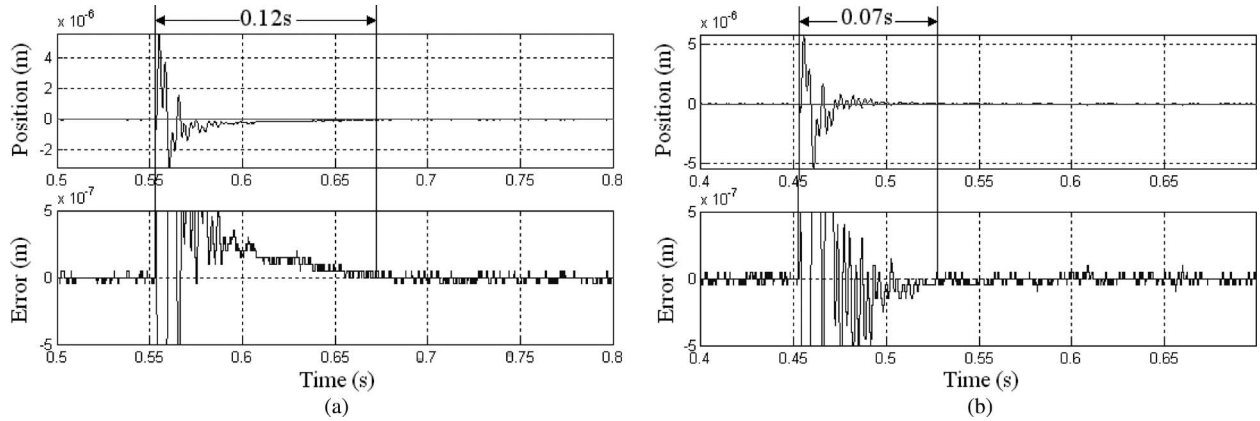

Fig. 14. Experimental results of controlled PMLM by standard IMRC algorithm (with impulse contact force disturbance).

position command is changed, the I_s becomes a large value, and this does not happen in the minimum step response.

Based on the information from the error–time graph in Fig. 13(a), the unexpected overshoot appears despite the fact that the critical damping model is used. The time-delay properties of LPF in disturbance compensator possibly cause this small overshoot. The excessive and delayed compensation current develops extra thrust force in the translator and produces the small overshoot.

Referring to the impulse disturbance response shown in Fig. 14(a), the settling time is 0.12 s, and it is a long time from the industrial application view. This slow response is due to the fact that the disturbance compensator requires a long time to accumulate the $I'_{\rm cmp}$ to overcome the static friction and cogging force.

To conclude, the original disturbance compensation system and standard IMRC system can also achieve the submicrometer precision linear motion system. The problem of this nonmodified approach is because the nonlinear static friction lengthens the settling time and causes a slow operating speed. Note that these results are shown for comparison with the performance of the new proposed method.

D. Modified Disturbance Compensation

Inserting K_i can improve the transient response of the position output, such as reducing the rising time and improving the response time to the disturbances in the PMLM. However, K_i should not be too large in order to prevent amplifying the effects of noise in I_s and the serious oscillation appearing at

TABLE II
PERFORMANCE OF CONTROLLED COMPENSATED PMLM WITH DIFFERENT K_i

	Rising time (s)				Steady state error deviation (nm)				Overshoot (%)			
Input step size	K_i=1	K_i=1.5	K_i=2	K_i=2.5	K_i=1	K_i=1.5	K_i=2	K_i=2.5	K_i=1	K_i=1.5	K_i=2	K_i=2.5
100nm	0.116s	0.096s	0.082s	0.07s	100	100	100	150	0	0	0	0
200nm	0.113s	0.092s	0.074s	0.067s	100	100	100	150	0	0	0	0
500nm	0.104s	0.086s	0.072s	0.065s	100	100	100	150	0	0	0	0
1μm	0.096s	0.081s	0.069s	0.063s	100	100	100	150	5	5	5	5
2μm	0.076s	0.064s	0.059s	0.057s	100	100	100	200	5	5	5	5
5μm	0.057s	0.052s	0.051s	0.05s	100	100	100	200	4	3	3	2
10μm	0.048s	0.046s	0.046s	oscillate	100	100	100	oscillate	2.5	2	2	oscillate
20μm	0.048s	0.05s	oscillate	oscillate	100	100	oscillate	oscillate	1.25	1	oscillate	oscillate
50μm	0.056s	0.056s	oscillate	oscillate	100	100	oscillate	oscillate	0.5	0.4	oscillate	oscillate

the position output. Before the profile of K_i is determined, some experiments had been conducted in order to investigate the effect of K_i. The compensated PMLM controlled by IMRC is commanded to travel with different position step command. The rising time, steady-state error deviation, and the overshoot level were studied. The results are summarized and shown in Table II.

The value of K_i can cause the performances of the compensated PMLM to change. When K_i is increased, the rising time of the step response is reduced. This is exactly predicted as shown in Section III-B. The additional terms $[1 - F(s)] \times [I_s K_f (K_i - 1)]$ in (7) can improve the response time by using K_i larger than one. At the same time, when K_i is larger than two, the steady-state error deviation is larger. It is because the filter $1 - K_i F(s)$ acts as an amplifier when K_i is equal to and larger than two (as shown in Fig. 4). This amplifier enlarges the external disturbance, variations in parameters, and the kinetic friction and increases the error deviation. One of the improvements of K_i, which is not expected, is the reduction in overshoot, although the effect of improvement is very small. This could be because $[1 - F(s)] \times [I_s K_f (K_i - 1)]$ in (7) amplifies the high-frequency component in I_{cmd} and the system can react to the position error quicker than the conventional disturbance compensator.

The PMLM will oscillate when K_i is large. When K_i is larger than two, the position error (equal to the amplitude of input step) is large. It must be prevented by defining the profile of K_i deliberately.

The improvement in rising time is not significant when the step size (position error) is larger than 20 μm. K_i is chosen to be two when the position error is smaller than 20 μm. Although there is no experimental study on the relationship between K_i and the velocity, a large K_i is expected to be utilized when the static friction is present. K_i should be two only when the velocity is small (i.e., $K_i = 2$ when the speed is 1 mm $\cdot$ s^{-1}, within one resolution of velocity measurement).

The profile of K_i is shown in Fig. 15. The shape of K_i is determined by experiments, and this arrangement is treated as optimum setting, which does not amplify the noise in I_s and which improves the response time of the PMLM effectively. The K_i varying mechanism was implemented to the compensated PMLM with IMRC algorithm. The step response experiments (with square wave input with minimum step size and critical condition step size) were conducted in order to illustrate the success of the proposed algorithm. The results are shown in Figs. 12(b) and 13(b).

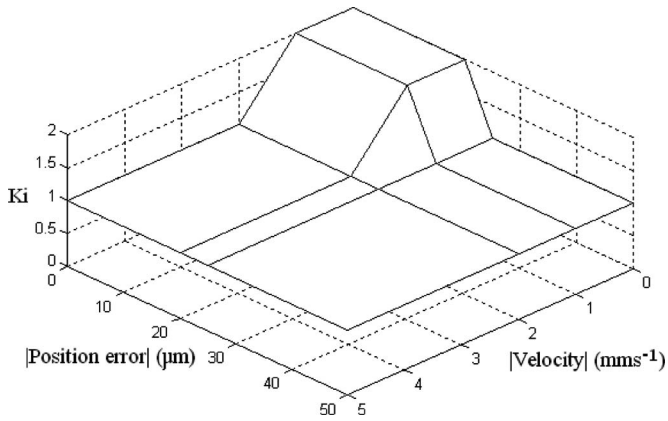

Fig. 15. Lookup table for K_i.

Based on the experimental results, the performance of the controlled PMLM with varying K_i mechanism is better than that of the original control algorithm. Considering the two position–time graphs in Figs. 12 and 13, the response time of the positioning system with K_i varying mechanism is smaller than that of the original control algorithm. In Fig. 12, the response time reduces from 0.116 to 0.082 s. In Fig. 13, the response time reduces from 0.067 to 0.056 s. Another valuable observation is related to the recovery time after the overshoot. Referring to the error–time graphs in Fig. 13, after the occurrence of overshoot, the controlled PMLM with varying K_i mechanism can bring the translator back to set point faster than using the controlled PMLM with original algorithm. The varying K_i mechanism not only reduces the rising time of the position of PMLM but also can maintain the precision and accuracy of the position output (steady-state error is $\pm$50 nm).

To investigate the response time toward the disturbance, an impulse disturbance was applied to the controlled compensated

PMLM with K_i varying mechanism. The disturbance response is plotted as shown in Fig. 14(b). The experimental results illustrate that the disturbance recovery time is improved from 0.12 to 0.07 s. As mentioned before, the long settling time shown in Fig. 14(a) is caused by static friction. This experimental result also proves that the effect of static friction can be reduced by using varying K_i mechanism.

The largest step response of the experiments is 800 μm, but it is not the traveling range limitation of the proposed system. If the profile of the position command is designed properly, the traveling range of the proposed mechanism can be longer. For example, the derivative and double derivative of position command can be controlled (the velocity command and the acceleration command) so that the corresponding input current I_s can be limited within 3 A and the velocity of PMLM can be limited within the maximum measurable speed of the optical linear incremental encoder (0.35 m $\cdot$ s^{-1}).

VI. Conclusion

A general-purpose PMLM is being controlled for developing a submicrometer precision linear motion system. The control strategy includes a modified disturbance observer and compensator, and the IMRC algorithm. The external disturbance, the effect of parameter uncertainties, and the frictional force can be eliminated effectively, and the position of the motor could be tracked precisely.

The two main contributions of this paper are "establishing the method to optimize g_f in the LPF of the disturbance observer" and "introducing the additional gain K_i to modify the performance of the conventional disturbance observer." The design additional gain K_i is the major contribution of this paper, and the effect of the static friction is reduced by the presence of K_i. Referring to the experimental results, the PMLM can be driven with the minimum step equal to 0.2 μm, with error deviation equal to 0.1 μm and with shorter response time.

References

[1] Y. Park, "Precision motion control of a three degrees-of-freedom hybrid stage with dual actuators," *IET Control Theory Appl.*, vol. 2, no. 5, pp. 392–401, Jul. 2007.

[2] S. Seshagiri, "Position control of permanent magnet stepper motors using conditional servocompensators," *IET Control Theory Appl.*, vol. 3, no. 9, pp. 1196–1208, Jun. 2008.

[3] R. Cao and K. S. Low, "A repetitive model predictive control approach for precision tracking of a linear motion system," *IEEE Trans. Ind. Electron.*, vol. 56, no. 6, pp. 1955–1962, Jun. 2009.

[4] Y. S. Huang and C. C. Sung, "Function-based controller for linear motor control systems," *IEEE Trans. Ind. Electron.*, vol. 57, no. 3, pp. 1096–1105, Mar. 2010.

[5] Y. Hong and B. Yao, "A globally stable high-performance adaptive robust control algorithm with input saturation for precision motion control of linear motor drive systems," *IEEE/ASME Trans. Mechatronics*, vol. 12, no. 2, pp. 198–207, Apr. 2007.

[6] C. C. Sung and Y. S. Huang, "Based on direct thrust control for linear synchronous motor systems," *IEEE Trans. Ind. Electron.*, vol. 56, no. 5, pp. 1629–1639, May 2009.

[7] L. Bascetta, P. Rocco, and G. Magnani, "Force ripple compensation in linear motors based on closed-loop position-dependent identification," *IEEE/ASME Trans. Mechatronics*, vol. 15, no. 3, pp. 349–359, Jun. 2010.

[8] S. L. Chen, K. K. Tan, S. Huang, and C. S. Teo, "Modeling and compensation of ripples and friction in permanent-magnet linear motor using a hysteretic relay," *IEEE/ASME Trans. Mechatronics*, vol. 15, no. 4, pp. 586–594, Aug. 2010.

[9] W. Yao, P. Tung, C. C. Fuh, and F. C. Chou, "A robust uncertainty controller with system delay compensation for an ILPMSM system with unknown system parameters," *IEEE Trans. Ind. Electron.*, vol. 58, no. 10, pp. 4727–4735, Oct. 2011.

[10] Y. P. Zhang, C. M. Akujuobi, W. H. Ali, C. L. Tolliver, and L. S. Shieh, "Friction compensation of an XY feed table using friction-model-based feedforward and an inverse-model-based disturbance observer," *IEEE Trans. Ind. Electron.*, vol. 56, no. 10, pp. 3848–3853, Oct. 2009.

[11] S. Komada, M. Ishidar, K. Ohnishi, and T. Hori, "Disturbance observer-based motion control of direct drive motors," *IEEE Trans. Energy Convers.*, vol. 6, no. 3, pp. 553–559, Sep. 1991.

[12] R. Krishnan, *Electric Motor Drives—Modeling, Analysis, and Control*. Upper Saddle River, NJ: Prentice-Hall, 2001.

[13] K. C. Kim, Y. M. Choi, J. J. Kim, and D. G. Gweon, "Development of control algorithm to reduce force ripple for high speed Permanent Magnet Linear Motor (PMLM)," in *Proc. Int. Conf. Control, Autom. Syst.*, Seoul, Korea, Oct. 17–20, 2007, pp. 1712–1716.

[14] D. L. Zhang, Y. P. Chen, Z. D. Zhou, W. Ai, and X. D. Li, "Robust adaptive motion control of permanent magnet linear motors based on disturbance compensation," *IET Electron Power Appl.*, vol. 1, no. 4, pp. 543–548, Jul. 2007.

[15] K. S. Low and M. T. Keck, "Advanced precision linear stage for industrial automation applications," *IEEE Trans. Instrum. Meas.*, vol. 52, no. 3, pp. 785–789, Jun. 2003.

[16] S. Katsura, K. Irie, and K. Ohishi, "High precision force control by multi-sensor based disturbance observer," in *Proc. 32nd IEEE IECON*, 2006, pp. 5227–5233.

[17] K. K. Tan, T. H. Lee, H. Dou, and S. Huang, *Precision Motion Control—Design and Implementation*. Berlin, Germany: Springer-Verlag, 2001.

[18] A. Datta and L. Xing, "The theory and design of adaptive internal model control schemes," in *Proc. Amer. Control Conf.*, Jun. 1998, pp. 3677–3684.

[19] D. E. Rivera, "Internal model control: A comprehensive view," Dept. Chem., Bio Mater. Eng., College Eng. Appl. Sci., Arizona State Univ., Tempe, AZ, 1999.

[20] M. Morari and E. Zafiriou, *Robust Process Control*. Englewood Cliffs, NJ: Prentice-Hall, 1989.

Hoi-Wai Chow (M'09) was born in Hong Kong in 1985. He received the B.Eng. degree in electrical engineering from The Hong Kong Polytechnic University, Hung Hom, Hong Kong, in 2007.

Since then, he has been with the Power Electronic Laboratory, The Hong Kong Polytechnic University, working on the low-cost submicrometer displacement sensor and high-precision control.

Norbert C. Cheung (SM'05) received the B.Sc. degree from the University of London, London, U.K., in 1981, the M.Sc. degree from the University of Hong Kong, Pokfulam, Hong Kong, in 1987, and the Ph.D. degree from the University of New South Wales, Kensington, Australia, in 1996.

He is currently an Associate Professor with the Department of Electrical Engineering, The Hong Kong Polytechnic University, Hung Hom. He has published more than 30 journal papers and more than 70 conference papers. He has also obtained three patent inventions. His research interests include mechatronics, instrumentation, control, industrial electronics, motors, and actuators.